 CMC, vol.20, no.2, pp.185-203, 2010

Experimental and Numerical Investigation on the Size of Damage Process Zone of a Concrete Specimen under Mixed-Mode Loading Conditions

X.P. Shen[1] and J.L. Feng[2]

Abstract: The characteristic length of a gradient-dependent damage model is a key parameter, which is usually regarded as the length of damage process zone (DPZ). Value and evolution of the size of DPZ were investigated by both a numerical method and an experimental manner. In the numerical study, the geometrical model adopted was a set of four-point shearing beams; the numerical tool used was the Abaqus/Explicit software. The distance between the front and end of a complete DPZ was obtained. Values of strain components at these points were given out at given time points. The experimental study of the evolution process of a damage process zone was investigated with a set of concrete specimens under mixed-mode loading conditions by using a white-light speckle method. The geometrical parameters of the damage process zone were measured. Double-notched specimens under four-point shear loading conditions were adopted. A series of displacement fields for points on the surface of the specimen were measured and further transferred into a strain field of these points during loading process. With reference to the strain values that occurred at both the front and end of a numerically-obtained DPZ, the length of the DPZ was determined with the experimental results.
These results provide an experimental basis for the determination of the value of an internal length parameter for a gradient-enhanced and/or area-averaged non-local model.

Keywords: Concrete, damage, plasticity, process zone, characteristic length, white-light speckle method.

1 Introduction

Owing to the heterogeneous material property of concrete-like materials, non-local inelastic models are becoming increasingly popular in dealing with fracture and

[1] Halliburton Energy Services, Houston, TX, U.S.A.
[2] Tsinghua University, Beijing, China.

damage of concrete structures (Bazant and Pijaudier-Cabot 1988; Aifantis 1992 and 2003; Saanouni, Chaboche, and Lesne 1988). Internal length is an important parameter of a gradient-enhanced, non-local damage model and of an area-averaged, non-local model. In a gradient-enhanced, non-local model, see Aifantis (1992), the internal length is the parameter that controls influence of its gradient enhancement term. In an area-averaged, non-local model, the internal length is the parameter that defines the scope of averaging calculation.

However, the definition of the internal length for a non-local model for concrete-like material has never been uniquely given, and consequently, the calibration of internal length has not been effectively investigated. The damage process zone (DPZ) is the region where material degradation occurs before macro fracture appears for concrete-like quasi-brittle materials. Bazant and Cedolin (1991) regarded the length of the DPZ as the internal length but did not explicitly give its value. Some researchers even believe the width of crack occurred within a structure is its internal length. For the gradient-enhanced damage model, Shen, Shen, and Chen (2005) took the internal length as the parameter that indicates the influence of the damage-gradient enhancement term on the non-local behavior and proposed its value in a manner of phenomena-match. Although quite a few researchers have been using the concept of internal length, few have made any explicit statement on the determination of its value.

With reference to the principle of 'non-local energy dissipation,' for concrete-like materials, it is believed here that the internal length of a gradient-enhanced damage model should be the length of the DPZ because the damage process at points within the same DPZ can influence each other, and it will not be influence by the energy value outside this damage process zone. Consequently, the length of a DPZ can represent the influence scope of a damage process, and, thus, it should be regarded as the internal length of a non-local damage model. The goal of this study is to experimentally measure the length of the maximum DPZ with a double-notched, four-point shear concrete beam.

The white-light speckle method is an experimental measure, which is widely used for surface deformation measuring purposes. With this method, the in-plane displacement field can be recorded at every time point within a given time interval. The related strain field can be calculated on the basis of the difference of the displacement field by comparing two displacement fields at different time points.

The white-light speckle method can record the displacement field and derive the related strain field occurring on the surface of a specimen; however, it cannot measure the damage process, which is 'hidden' and is in front of a macro fracture. The damage process can only be calculated numerically with a set of given elastoplastic damage constitutive relations. The elastoplastic damage constitutive model used here is the one proposed by Lubliner, Oliver, Oller, and Onate (1989) and further developed by Fenves and Lee (1998).

In the following sections, experiments performed with the white-light speckle method and four-point shear will be introduced first. Numerical results obtained with finite-element analysis will be presented afterwards. Comparisons of the experimental results with the numerical results will be done subsequently. Conclusions will be made at the end.

2 Experiments performed with the white-light speckle method and four-point shear beam

2.1 Testing device

The testing system is shown in Fig. 1. A concentrated loading force, P, is applied on the loading beam, which is made of steel. Force, P, is applied on the concrete specimen through two rollers, which are set in a way to redistribute it into force P1 and force P2 at the roller positions, with P2 equals to P1/15. P1, together with the reaction force at the inside supporting roller, will form a narrow shearing region within, where material points will be mainly at a shear-stress state. The geometrical parameters of the specimen are: height of 150 mm, length of 400 mm, and the width of the notch is 5 mm with a depth of 25 mm. The horizontal distance between P1 and the contact point of right supporting roller is 25 mm, and the distance from the contact point between the left supporting roller and the left edge of specimen is 12.5 mm.

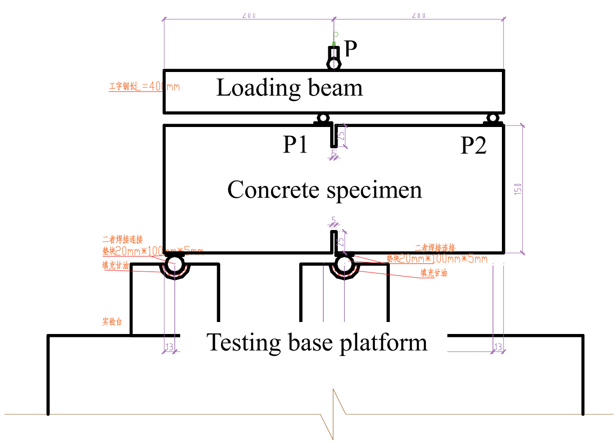

Figure 1: Geometry of loading system.

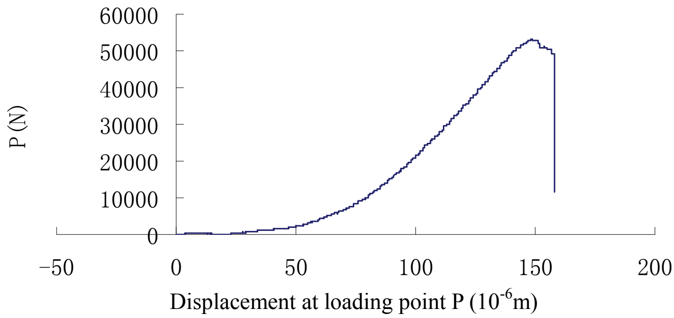

Figure 2: Diagram of loading force versus displacement at loading point P.

2.2 *Experimental results*

The displacement-force diagram of the full-loading process is shown in Fig. 2. The total process has been recorded by 13,500 digital photos. The camera speed is 15 pictures per second. Four selected resultant pictures of maximum shear strain, γ_{max}, are shown in Fig. 3. These figures of strain were calculated in terms of the displacement field recorded by the white-light speckle method. The range of the localization zone of the shear strain (i.e., shear band) has been indicated in Fig. 3 corresponding to various loading time steps.

Fig. 3(a) was taken at the stage that had no obvious damage and strain localization. Fig. 3(b) was taken at the stage in which the localization band had just been formed. Fig. 3(c) was taken at the moment that macrofracture was just formed. Fig. 3(d) illustrates the moment when secondary DPZ was formed. As discussed before, although there are obvious localization bands formed within the specimen, it is not possible to tell where the DPZ starts and ends without reference to a specific plastic damage constitutive model. This problem will be solved in the following section using finite-element analysis and the specific damage model proposed by Lubliner, Oliver, Oller; Onate (1989) and further improved by Lee and Fenves (1998).

3 Numerical results obtained with finite-element analysis

In the numerical study, two models were used: the first modeled is the four-point, double-notched shear beam, and the second model is the single-notched, four-point shear beam. The parameters for the double-notched beam are the same as the specimen used in the experiment mentioned above, and it is used to compare with the results obtained by specimen testing. The model of single-notched, four-point beam is used to see the variation of the geometrical character of a DPZ with a different

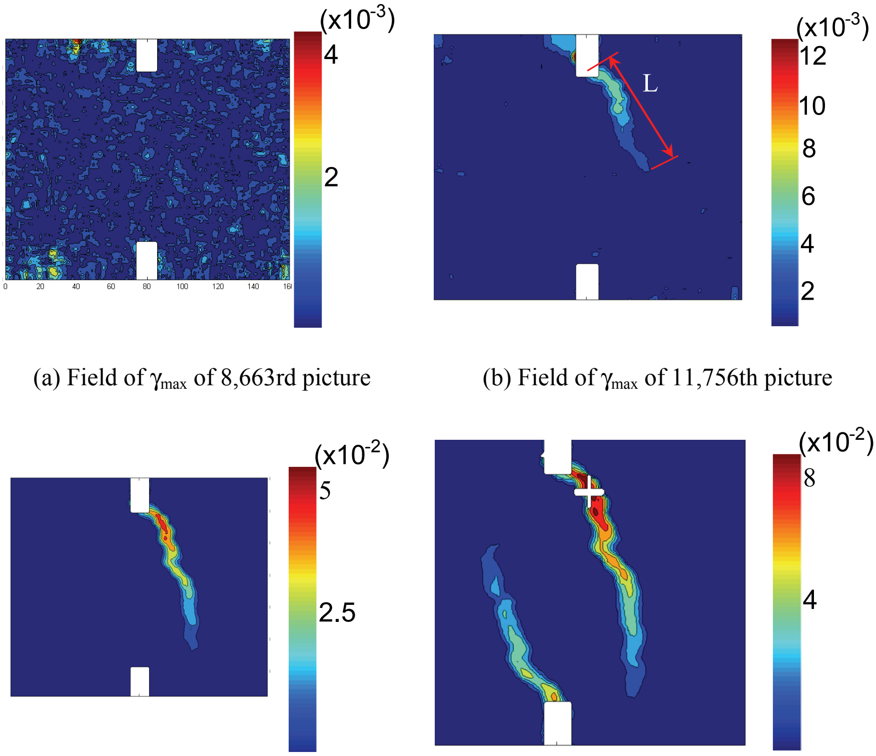

(a) Field of γ_{max} of 8,663rd picture

(b) Field of γ_{max} of 11,756th picture

(c) Field of γ_{max} of 12,828th picture;

(d) Field of γ_{max} of 13,186th picture

Figure 3: Evolution of field of γ_{max} and damage process zone.

specimen.

3.1 Discretization of the double-notched, four-point shear beam

Th mesh of the double-notched, four-point shear beam used in the test is shown in **Fig. 3**. Numerical simulation was done with ABAQUS/Explicit. In the following, numerical results of damage and strain at time t=1.25 s, 1.475s, and 1.4875 were chosen and analyzed so as to illustrate the process of damage initiation and evolution. A DPZ is the area in which damage values at material points in this region vary from close to 0 to 1. In the process of loading in the study, at time t=1.25 s, it is the moment of damage initiation; at time t=1.475 s, it is the moment of occurrence of a complete damage process zone; and at time t=1.4875 s, it is the moment when a complete damage process zone moves.

It should be noted that because the loading speed used in the numerical simulation is not exactly the same as the one used in test with specimen, consequently, the time point taken in numerical calculation does not match the time moment with the same time value, t.

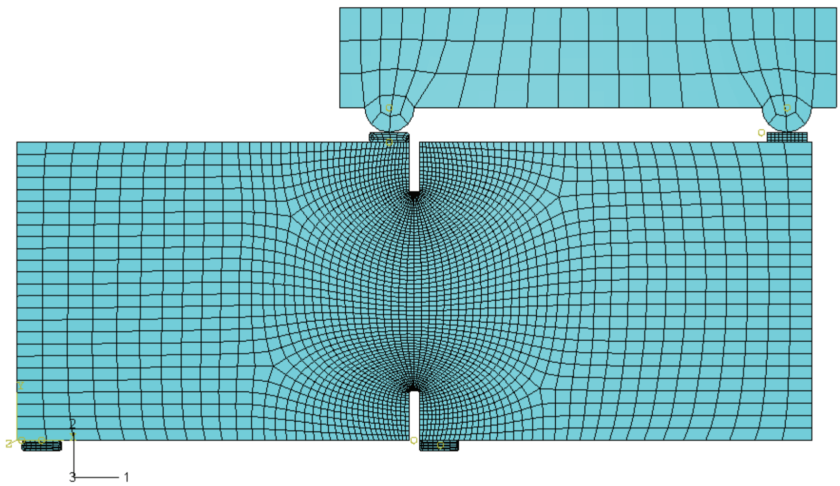

Figure 4: Mesh of the model.

3.2 Numerical results obtained with double notched beam.

3.2.1 Distribution of damage and strain at t=1.25 s.

In Figs. 5 through 8, the strain components, ε_{11}, ε_{22}, ε_{12}, and damage variable, D, localize into a narrow band, as illustrated in bright color. There is only a localization band in the structure at the moment.

As shown in Fig. 8, Path AB is chosen, and damage and strain variables along path AB will be illustrated in Figs.9–12 for time t=1.25s. As shown in Fig. 9, the maximum value of damage is 0.8, and, thus, a complete damage process has not been formed yet. When comparing Fig. 10 with Fig. 12, it is found that the maximum shear strain is 0.0057 and the maximum normal strain is 0.0048, which indicates that it is shear-dominated deformation at the moment t=1.25s.

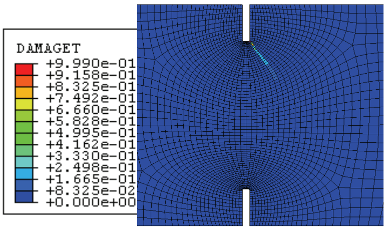

Figure 5: Distribution of tensile damage, t=1.25s.

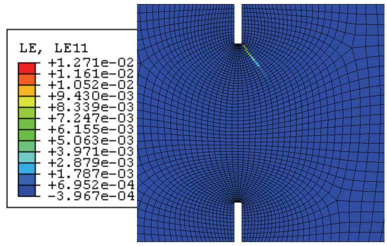

Figure 6: Distribution of tensile strain component, ε_{11}, t=1.25s.

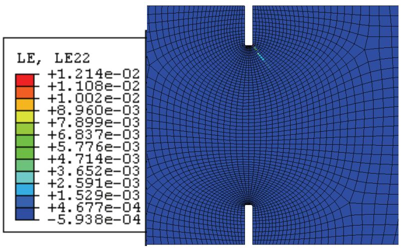

Figure 7: Distribution of tensile strain component,ε_{22}, t=1.25s.

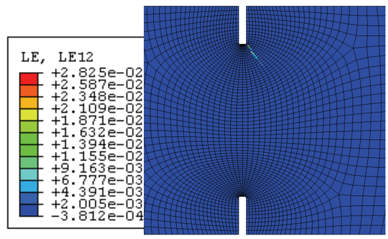

Figure 8: Distribution of tensile strain component, ε_{12}, t=1.25s.

3.2.2 Distribution of damage and strain at t=1.475 s.

Figs. 13 through 16 show the distributions of damage, D, and strain components within the newly-formed complete damage process zone. There is only one band of localization of damage.

Figs. 17 through 19 illustrate the distributions of damage, D, and strain components along Path AB. In Fig. 17, the maximum value of damage reaches 1, which indicates an occurrence of complete damage process zone. When comparing Fig. 18 with Fig. 19, it is found that value of maximum shear strain is 0.037, and the value of maximum normal strain is 0.007 at the end of the damage zone, which indicates that the deformation at the moment is shear-dominated. The front of the damage process zone has 0 damage, as shown in Fig. 17. The shear strain in Fig. 19 is 0.000088, and the normal strain in Fig. 18 is 0.00095, which is 10 times the shear strain. This shows that deformation at the front point of the damage process zone at the moment is tension-dominated.

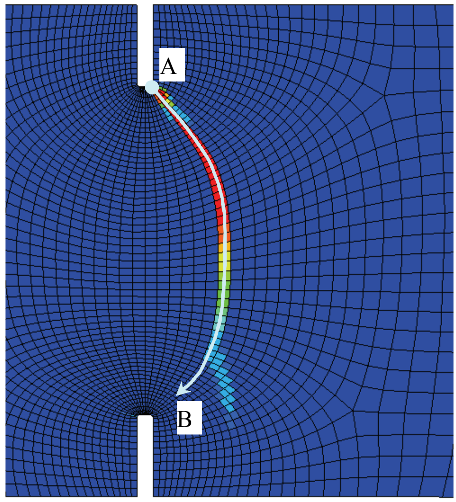

Figure 9: Path AB along which band of damage localization develops.

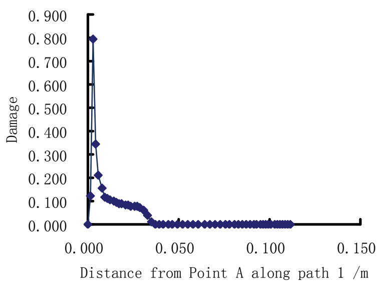

Figure 10: Distribution of damage D along Path AB, t=1.25 s.

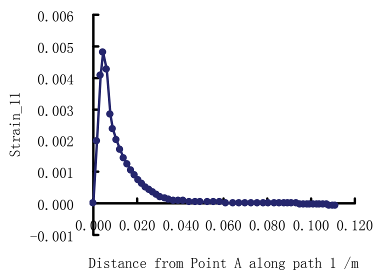

Figure 11: Distribution of strain component ε_{11} along path AB at t=1.25 s.

3.2.3 *Distribution of damage and strain at t=1.4875*

Figs .20–22 illustrate the distributions of damage, D, and strain components, ε_{11} andε_{12}, within specimen. These Figs illustrate development and movement of the complete damage process zone under mixed-mode loading. In Fig. 20, it is seen that the complete damage process zone develops along path AB and bifurcates at a point near point B. A secondary damage zone just starts to form in the left corner of the lower notch close to B, but not so obvious yet.

The distribution of damage, D, and strain components at time t=1.4875 s along Path

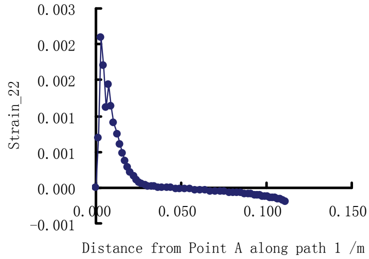

Figure 12: Distribution of strain component ε_{22} along path AB at t=1.25 s.

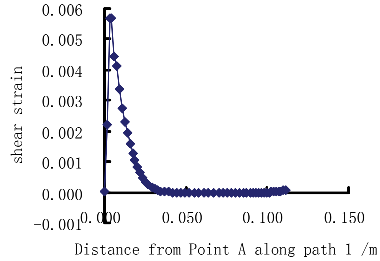

Figure 13: Distribution of strain component ε_{12} along path AB at t=1.25 s.

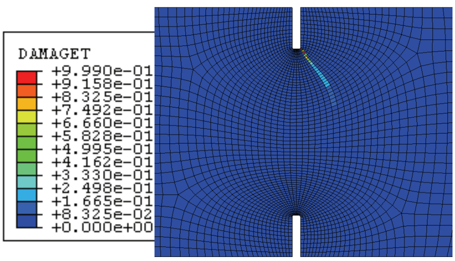

Figure 14: Distribution of damage, D, at t=1.475 s.

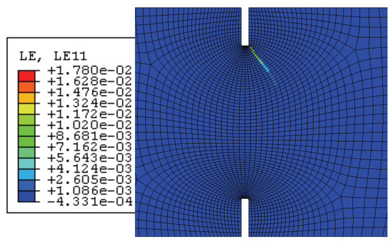

Figure 15: Distribution of strain component, ε_{11}, at t=1.475 s.

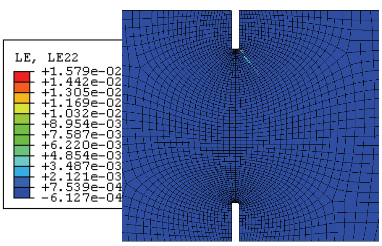

Figure 16: Distribution of strain component, ε_{22}, at t=1.475 s.

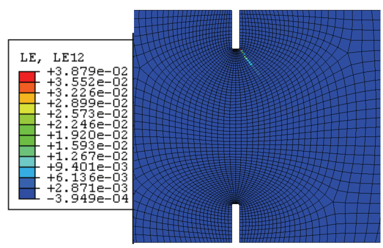

Figure 17: Distribution of strain component, ε_{12}, at t=1.475 s.

AB are shown in Figs. 23–25. By comparing Fig. 24 with Fig. 25, it is found that the maximum value of shear strain at the tail of damage process zone is 0.0675, and that of tensile strain is 0.05. It indicates that the deformation is shear-dominated. In Fig. 23 and Fig. 24, it is shown that at the front of the damage process zone, the

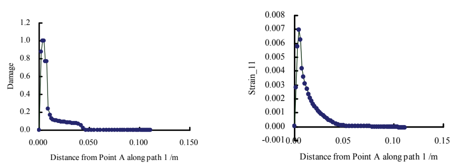

Figure 18: Distribution of damage, D, along Path AB at t=1.475 s.

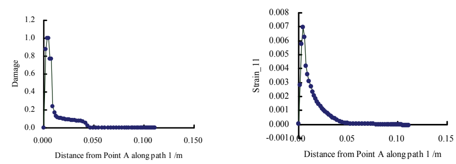

Figure 19: Distribution of strain, ε_{11}, at t=1.475 s.

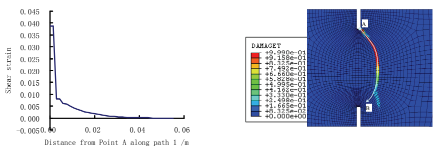

Figure 20: Distribution of strain, ε_{12}, at t=1.475 s.

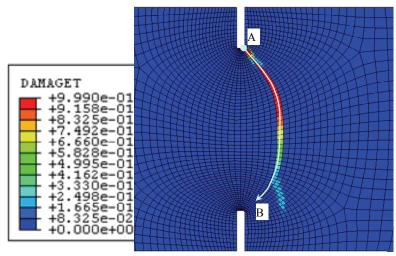

Figure 21: Distribution of damage, D, at t=1.4875 s.

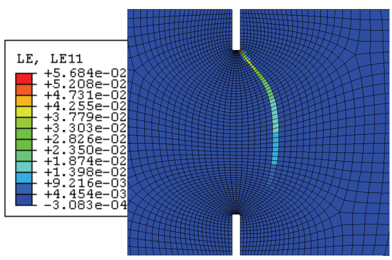

Figure 22: Distribution of strain component, ε_{11}, at t=1.4875 s.

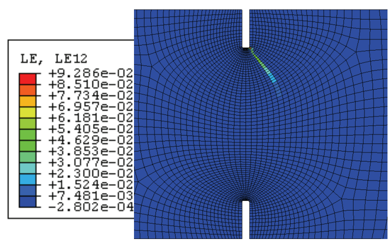

Figure 23: Distribution of strain component, ε_{12}, at t=1.475 s.

maximum value of tensile strain is 0.00065, and the shear strain in Fig. 25 at this position is -0.000088, which is less than 1/7 of the tensile strain. It indicates the deformation here is normal strain-dominated.

The length of the damage process zone is the shortest distance between the point with damage value 1 and the point with damage value 0.

In the following, Table 2 lists values of damage and strain components at both the front point and end point of the damage process zone at time=1.475 s. Values of the aforementioned variables at time t=1.4875 s are listed in Table 3.

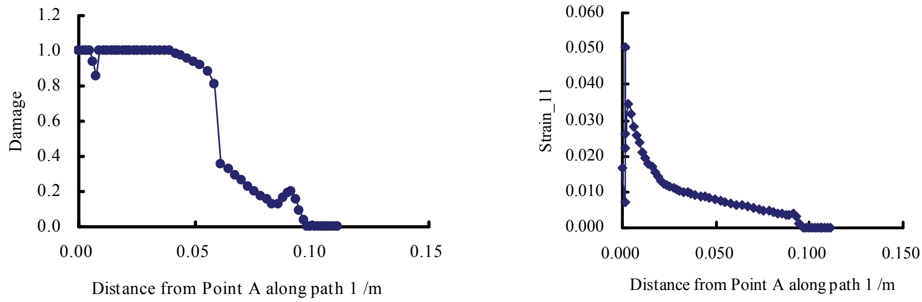

Figure 24: Distribution of damage, D, along Path AB at t=1.4875 s.

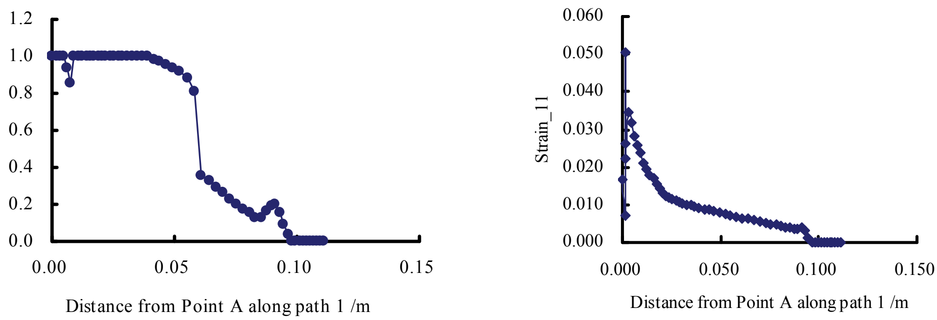

Figure 25: Distribution of strain, ε_{11}, along Path AB at t=1.4875 s.

Table 2 shows that the length of damage process zone at t=1.475 s is 0.0421 m. Table 3 shows that the length of the damage process zone at t=1.4875 s is 0.0612m.

Table 1: Values of damage and strain at both ends of a complete DPZ, t=1.475 s.

t=1. 475 s	Distance from Point A	damage	ε_{12}	ε_{11}	ε_{22}
At front of DPZ	4.66E-02	0	1.41E-05	9.46E-05	8.81E-06
At end of DPZ	4.57E-03	0.999	7.94E-03	6.96E-03	2.30E-03

The aforementioned results indicate that the size of the damage process zone is a variable, which depends on the stress status. With the development of stress status within the neighborhood of damage process zone, the size of DPZ varies, the size of DPZ under tension is different from the one under shear. Shen and Mroz (2000) have proven analytically that the size of DPZ for a mode-III fracture for a given

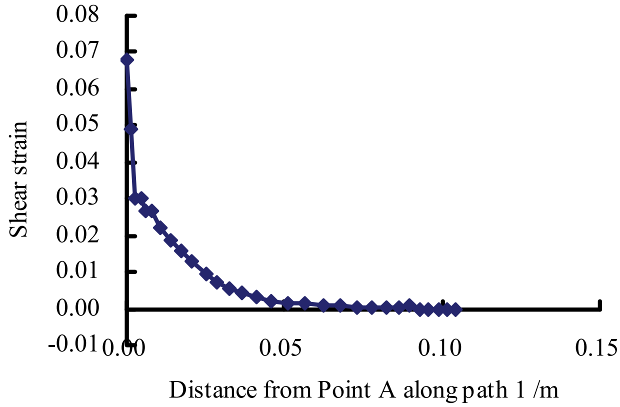

Figure 26: Distribution of strain, ε_{12}, along Path AB at t=1.4875 s.

Table 2: Values of damage and strain at both ends of a complete DPZ, t=1.4875 s.

t=1.4875 s	Distance from Point A	damage	ε_{12}	ε_{11}	ε_{22}
At front of DPZ	9.81E-02	0	-1.13E-04	5.51E-05	-1.13E-04
At end of DPZ	3.69E-02	0.999	4.22E-04	9.51E-03	4.22E-04

load is determined by 3 factors, which include stress tensor, material mechanical property (such as strength and Young's modulus, etc.), and geometry parameters.

3.2.4 Analysis on secondary DPZ.

As shown in Fig. 26, the secondary DPZ appears at the left upper corner of lower notch at time t=2.001 s after forming of complete the primary DPZ. As shown in Figs. 27–30, zoomed views of domain around the secondary DPZ visualize the appearance and development of the secondary DPZ, which follows a similar rule to that of the primary DPZ.

Distribution of damage, D, and strain components along Path CD in the domain of secondary DPZ are shown in Figs. 31–33. At time t=2.001s, the complete secondary DPZ appears when the damage value reaches 1 at its tail end.

Table 4 lists the values of damage and strain components at both ends of the secondary DPZ.

Table 4 shows that the size of the secondary DPZ is 0.0367 m.

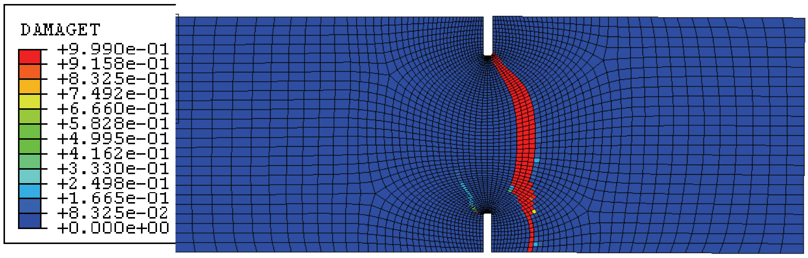

Figure 27: Onset of the secondary DPZ and its location within specimen.

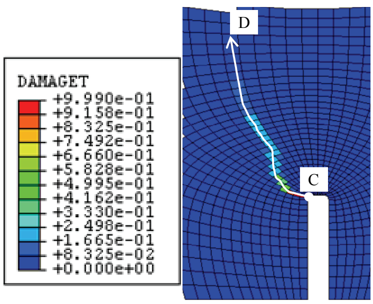

Figure 28: Zoomed view of the secondary DPZ.

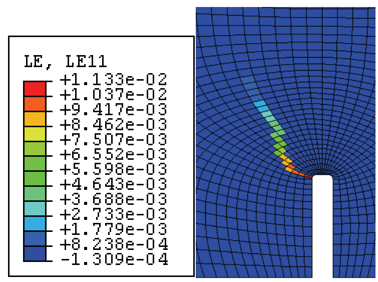

Figure 29: Zoomed view of distribution of strain, ε_{11}, around the DPZ.

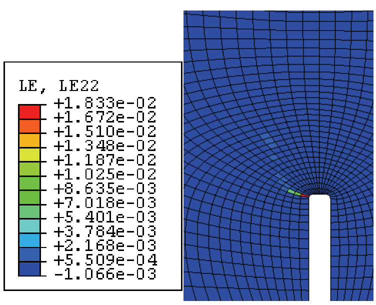

Figure 30: Zoomed view of distribution of strain ε_{22} around the DPZ.

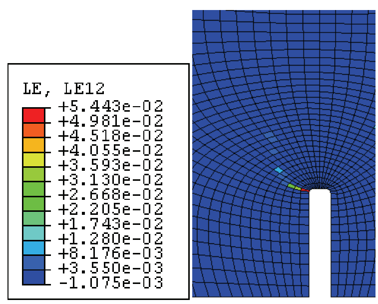

Figure 31: Zoomed view of distribution of strain γ_{12} around the DPZ.

3.3 Numerical results obtained with single-notched beam.

Keeping all the other conditions and parameters the same as the previous double-notched beam test, this test uses a single-notched beam specimen, which has a

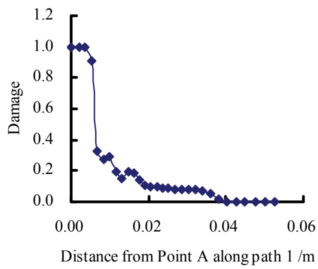

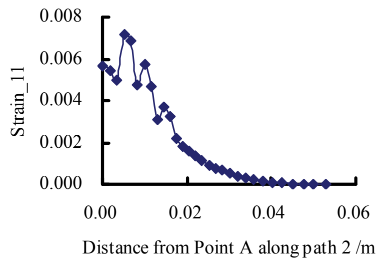

Figure 32: Distribution of damage, D, along Path CD.

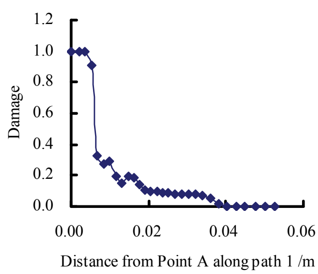

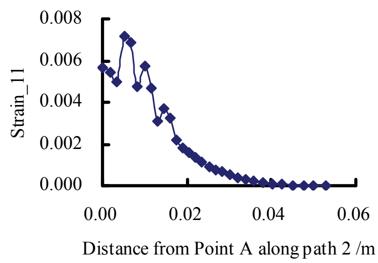

Figure 33: Distribution of strain component ε_{11} along Path CD.

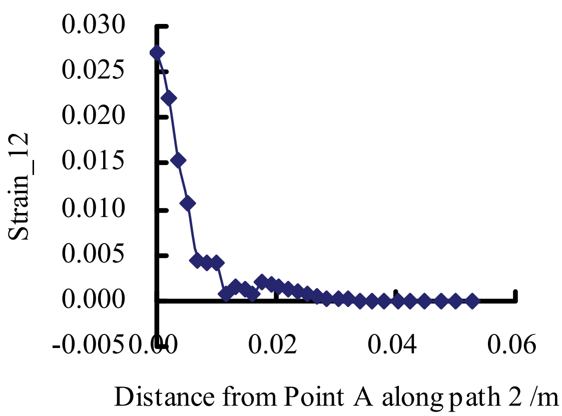

Figure 34: Distribution of strain component, ε_{12}, along Path CD.

Table 3: Values of damage and strain component at both ends of secondary DPZ, t=2.001 s.

t=2.001s	Distance from Point C	damage	ε_{12}	ε_{11}	ε_{22}
Front of secondary DPZ	4.02E-02	0	-7.09E-06	7.45E-05	1.76E-05
Tail of secondary DPZ	3.54E-03	0.999	1.53E-02	4.98E-03	3.84E-03

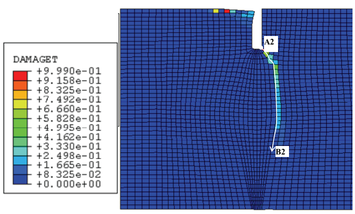

Figure 35: Distribution of damage, D, within the single-notched beam.

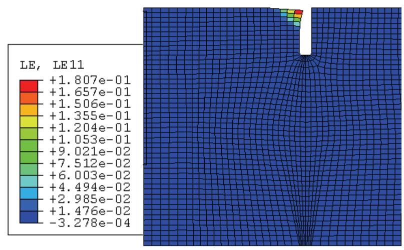

Figure 36: Distribution of strain, ε_{11}, within the single-notched beam.

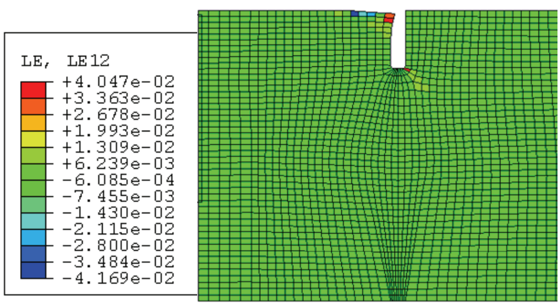

Figure 37: Distribution of strain component, ε_{12}.

length of 0.44 m and a height of 0.1 m. Numerical results for distribution of damage, D, and strain components at time t=1.5 s are illustrated in Fig. 34–37. Fig. 34 shows that a complete DPZ has appeared at this moment along Path A_2B_2.

Distribution of damage, D, and strain components along Path A_2B_2 are shown in Fig. 37–40. As shown in Fig. 38 and Fig. 39, the value of normal strain at the tail of the DPZ is 0.00797, and the value of shear strain is 0.0139, which indicates the deformation at this point is shear-dominated, mixed-mode deformation. At the front point of the DPZ, the value of normal strain is 0.000085, and shear strain is 0.00017, which indicates this point is also shear-dominated, mixed-mode deformation. The values of aforementioned variables are listed in Table-5.

Table 5 indicates that size of the DPZ for this test is 0.0473 m.

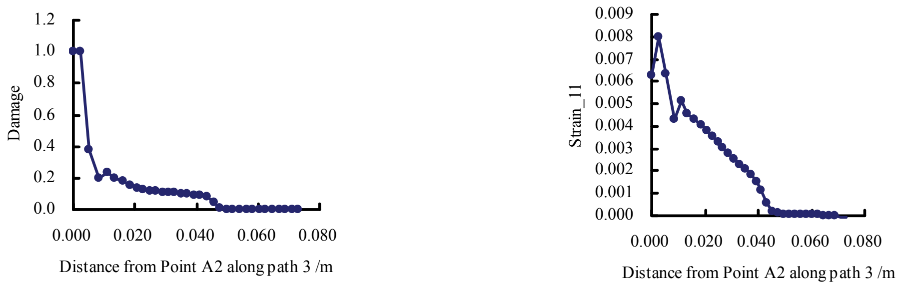

Figure 38: Distribution of damage, D, along Path A_2B_2.

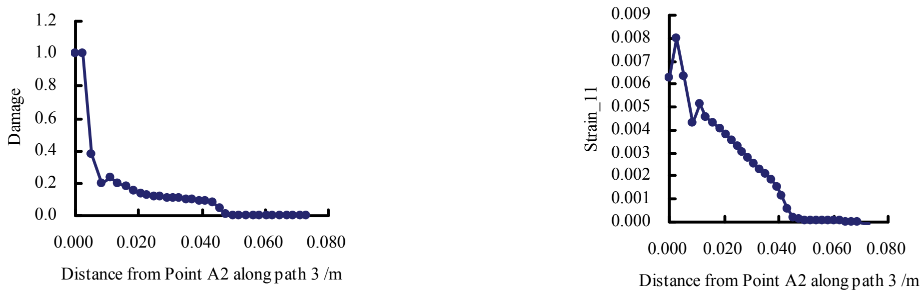

Figure 39: Distribution of strain, ε_{11}, along Path A_2B_2.

Table 4: Values of damage D and strain at both ends of DPZ.

Time t=1.5 s	Distance from A2	damage	ε_{12}	ε_{11}	ε_{22}
At front of DPZ	4.98E-02	0	1.07E-04	8.51E-05	4.70E-03
At tail of DPZ	2.52E-03	0.999	1.39E-02	7.97E-03	-1.01E-04

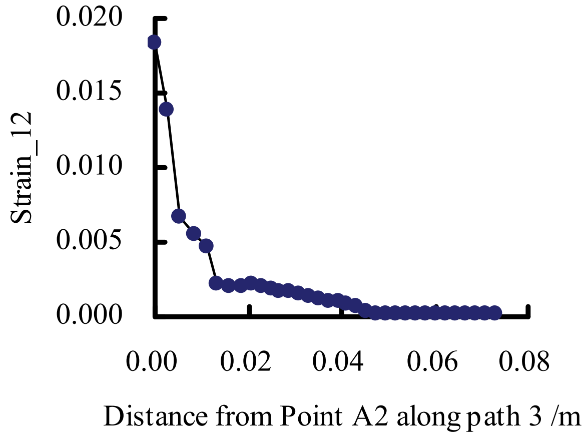

Figure 40: Distribution of strain, ε_{12}, along Path A_2B_2.

4 Comparisons of the experimental results with the numerical results

Because the loading condition is shear-dominated, maximum shear strain is taken as the reference valuable to calibrate the damage process zone. The damage process zone is determined through two critical strain values: γ_{c1}andγ_{c2}. Parameter,γ_{c1}, is the minimum strain value below which no damage will occur, and γ_{c2} is the maximum strain value above which damage will reach its limit 1, which corresponds to the initiation of macro-crack. The region has maximum shear-strain value continuously distributed between γ_{c1} and γ_{c2} will be regarded as damage process zone. This point has been numerically verified with the same values of γ_{c1} and γ_{c2} adopted here by the finite-element method.

From Table 2, it is found that $\gamma_{c2} = 0.00794$ for the end point of the DPZ with damage=1, and $\gamma_{c1} = 1.41 \times 10^{-5}$ for a front point of the DPZ with damage=0.

With these critical values of shear strain, from Fig. 2(b), the length of damage process zone can be determined approximately as $L = 0.054$m.

Another way that could roughly determine the values of γ_{c1} and γ_{c2} is to set these values with reference to the Young's modulus and cohesion of material of the specimen, and it will result in similar results for these two parameters.

5 Conclusions

In this study, a device of four-point shear beams was developed and used to calibrate the length of damage process zone. For the given size of a specimen, the length of the damage process zone was determined experimentally as $L = 0.054m$.

The length and evolution law of the DPZ of the concrete specimen have been studied numerically. Conclusions obtained include:

The length of a complete DPZ is in the range of 0.0421 m to 0.0612 m for the given specimen of double-notched beam with a height of 0.15 m and length of 0.4 m. The variation of the DPZ's length results from changes of stress status at points within DPZ. As distance becomes larger for a point from the notch, stress status varies from a shear-dominated status to a tension-dominated status.

Secondary DPZ will appear after occurrence of the complete primary DPZ. For the given specimen and loading, the length of its secondary DPZ is 0.0367 m.

For a single-notched beam given in this study, the length of its DPZ is 0.0473 m.

Comparisons have been made between numerical results and experimental results and are in good accordance. Trends of localization of strain and damage obtained from experiments are similar to those of numerical results; primary DPZ appears first and then comes the secondary DPZ.

The result of the length of damage process zone presented here has offered an experimental basis for determining the values of internal length, which is essential in a gradient-dependent damage model.

Acknowledgement: Financial support from Halliburton Energy Services is acknowledged gratefully. Partial financial supports from China National Natural Science Foundation through contract 10872134 and support from Liaoning Province through contract 2008RC38 are gratefully acknowledged.

References

Aifantis, E.C. (1992): On the role of gradient in the localization of deformation and fracture. Int. J. Engng. Sci. Vol. 30, pp.1279-1299.

Aifantis, E.C.(2003): Update on a class of gradient theories. Mech. of Mater., Vol. 35, no. 1, pp.259-280.

Bazant, Z. P. and Cedolin, L. (1991): S*tability of Structures: Elastic, Inelastic, Fracture And Damage Theories*, Oxford University Press, Oxford, New York.

Bazant, Z.P. and Pijaudier-Cabot, G. (1988): Nonlocal continuum damage, localization instability and convergence. ASME J. Appl. Mech., Vol. 55, pp.287-293.

Lee, J. and Fenves, G.L.(1998): A plastic-damage concrete model for earthquake analysis of dams. Earthquake Engng. Struct. Dyn. Vol. 27, pp. 937-956.

Lubliner, J.; Oliver, J.; Oller, S.; Onate, E. (1989): A plastic damage model for concrete. Int. J. Solids Struct., Vol. 25, no.3, pp. 299-326.

Saanouni, K.; Chaboche, J. L.; Lesne, P. M. (1988): Creep crack growth prediction by a non-local damage formulation, In: *Proceedings of Europe-US Workshop on Strain Localization and Size Effects in Cracking and Damage*, Cachan, 6-9 September 1988. (Edited by J. Mazars, Bazant, Z.P.). Elsevier Applied Science, London and New York, pp. 404-414.

Shen, X.; Mroz, Z. (2000): Shear beam model for interface failure under antiplane shear (I)-fundamental behavior. *Applied Mathematics and Mechanics: English Edition,* Vol.21, no.11, pp1221-1228

Shen, X.P.; Shen, G.X.; Chen, L.X. and Yang, L. (2005): Investigation on gradient-dependent nonlocal constitutive models for elasto-plasticity coupled with damage. Applied Mathematics and Mechanics-English Edition, Vol.26, No.2, pp. 218-234.